HHS Public Access

Author manuscript

Nat Struct Mol Biol. Author manuscript; available in PMC 2013 July 01.

Published in final edited form as:

Nat Struct Mol Biol. 2013 January ; 20(1): 90–98. doi:10.1038/nsmb.2460.

HLA-DO acts as a substrate mimic to inhibit HLA-DM by a competitive mechanism

Abigail I Guce[1,5], **Sarah E Mortimer**[1,5], **Taejin Yoon**[2,4], **Corrie A Painter**[1], **Wei Jiang**[2], **Elizabeth D Mellins**[2], and **Lawrence J Stern**[1,3]

[1]Department of Pathology, University of Massachusetts Medical School, Worcester, MA

[2]Department of Pediatrics, Stanford University, Stanford, CA

[3]Department of Biochemistry and Molecular Pharmacology, University of Massachusetts Medical School Worcester, MA

Abstract

MHCII proteins bind peptide antigens in endosomal compartments of antigen-presenting cells. The non-classical MHCII protein HLA-DM chaperones peptide-free MHCII against inactivation and catalyzes peptide exchange on loaded MHCII. Another non-classical MHCII protein, HLA-DO, binds HLA-DM and influences the repertoire of peptides presented by MHCII proteins. However, the mechanism by which HLA-DO functions is unclear. Here we use x-ray crystallography, enzyme kinetics and mutagenesis approaches to investigate human HLA-DO structure and function. In complex with HLA-DM, HLA-DO adopts a classical MHCII structure, with alterations near the alpha subunit 3_{10} helix. HLA-DO binds to HLA-DM at the same sites implicated in MHCII interaction, and kinetic analysis demonstrates that HLA-DO acts as a competitive inhibitor. These results show that HLA-DO inhibits HLA-DM function by acting as a substrate mimic and place constraints on possible functional roles for HLA-DO in antigen presentation.

The mammalian class II major histocompatibility (MHCII) locus includes genes for classical MHCII proteins that bind peptide antigens and present them to T cells, interspersed with genes for non-classical MHCII proteins that play accessory roles in the antigen loading process. The non-classical MHCII protein DM (HLA-DM in humans, H-2M or H2-DM in

Correspondence to: lawrence.stern@umassmed.edu.

[4]Current address, Department of Chemistry, Yonsei University, Seoul 120-749, Korea.

[5]These authors contributed equally to this work.

AUTHOR CONTRIBUTIONS

SEM prepared and crystallized the DMDO complex, SEM, AIG, and LJS interpreted diffraction data, AIG built the structural model, SEM performed kinetics experiments, TY, WJ, and AIG analyzed mutant proteins, AIG, SEM, TY, CAP, WJ, EDM and LJS designed experiments and analyzed data, AIG, SEM, CAP, WJ, EDM, and LJS wrote the manuscript.

COMPETING FINANCIAL INTERESTS

The authors declare no competing financial interests

ACCESSION CODES

Crystallographic data and atomic coordinates for the HLA-DO–HLA-DM complex are available from the Protein Data Bank with accession code 3USA.

mice) has a well-understood function in catalyzing peptide exchange on MHCII proteins [1,2]. MHCII proteins assemble in the endoplasmic reticulum with an invariant chain chaperone that occupies the peptide binding site and escorts bound MHCII to endosomal compartments, where the chaperone is degraded by endosomal proteases leaving a nested set of short peptides (CLIP) in the MHCII binding site [3]. DM acts to catalyze exchange of CLIP for endosomal peptides derived from endogenous proteins or endocytosed material [1]. The MHCII-peptide complexes traffic to the cell surface for inspection by CD4+T cells, as part of the system of antigen presentation and immune surveillance. In the absence of DM, many MHCII proteins do not exchange peptides and remain bound to CLIP, so that DM-deficient cells are defective in antigen presentation [4,5]. The molecular mechanism by which DM catalyzes peptide exchange on MHCII is not clear, but current ideas focus on stabilization of a MHCII-peptide intermediate with disrupted peptide main-chain hydrogen bonds or side-chain pocket interactions [6–10]. DM has another role in stabilizing peptide-free empty MHCII molecules against irreversible inactivation [2,11–13], presumably by binding to a peptide-free MHC II form and stabilizing a receptive conformation.

The other non-classical MHCII protein, DO (HLA-DO in humans, H-2O in mice) also plays a role in antigen presentation, although less well-defined than for DM. Expression of genes coding for MHCII, DM, and other proteins involved in MHCII antigen presentation are coordinately regulated by the class II transactivator CIITA, but DOβ has additional regulatory elements [14]. As a result, DO has a unique expression pattern, being expressed principally in B cells, thymic medullary epithelial cells, trophoblasts, and a subset of dendritic cells [15–17]. In B cells and dendritic cells, DO expression is developmentally regulated, with expression down-regulated as B cells enter germinal centers for affinity maturation and class switching [18,19] and as dendritic cells mature into fully-stimulating professional antigen presenting cells able to activate naïve T cells [16,20]. This expression pattern has suggested a role for DO in promoting tolerance to self-antigens [21,22], an idea supported by suppression of autoimmune diabetes in H-2O transgenic non-obsese diabetic (NOD) mice [23]. DO-knockout mice exhibit a different spectrum of MHCII-bound peptides than observed for DO-sufficient mice [24], and DO transfection alters the repertoire of MHCII-bound peptides in a human melanoma line [25]. Finally, antigen presentation function is altered in DO-deficient mice [24,26–28]. Antigens can access endosomal/lysosomal compartments for entry into the MHCII presentation pathway via fluid-phase endocytosis or receptor-mediated uptake. Studies with DO-deficient mice have shown that relative efficiency of MHCII presentation for these pathways is affected by DO, with DO typically promoting B-cell receptor-mediated uptake, although with differences observed for different epitopes and MHC II alleles[24,26–28].

On a molecular basis, most studies point to a role for DO in inhibiting DM function. *In vitro* experiments generally have shown that the DO–DM complex is inactive in catalyzing peptide exchange [25,29–31]. DO has been shown to block DM function in DO-transfected antigen presenting cells [29]. In addition, in mice over-expressing DO the cell surface level of MHCII-CLIP is increased [32], as it is in human DO transfectants [25], similar to the effect seen in DM-knockout cell lines and DM-deficient mice.

The three-dimensional structure of DO is not known, although it has been modeled based on homology to classical MHCII proteins [31,33]. In this work, we set to determine how DO modulates HLA-DM function. We determined the X-ray crystal structure of HLA-DO bound to HLA-DM and studied DO function through enzyme kinetics and mutagenesis studies. In the crystal structure, the DO and DM molecules bind in a side-by-side arrangement, similar to that that proposed for the complex of MHCII with DM. The DO–DM interface observed in the crystal structure is congruent with MHCII–DM interface predicted from mutagenesis studies, and DM mutants have similar effects on DO binding and MHCII-peptide exchange. Moreover, kinetic studies show that DO acts as competitive inhibitor of DM. Together, these results show that DO functions as a substrate mimic, by binding tightly to DM and preventing MHCII access. These results place constraints on potential functional roles for DO.

Results

DO inhibition of DM-mediated peptide binding and release

In vivo, DO forms a tight complex with DM [30]. In the absence of DM, DO is retained in the ER and degraded [30]. Because of this, most previous studies of DO function have focused on characterization of DODM complexes isolated from native or recombinant expression systems [25,29,34]. From a mechanistic point of view studies with isolated DODM complexes are limited because the concentrations of DM and DO could not be independently varied. For our studies we were able to prepare the extracellular domain of human DO independent of DM by expression in *Drosophila* S2 cells, using either an Ig-fusion protein (sDO-Fc) or C-terminal leucine-zipper (szDO) to stabilize the DO αβ heterodimer (Fig 1a). In some experiments, αP10a was mutated to Ala (termed szDOv), as a valine mutation at this position was previously reported to stabilize DO folding in the absence of DM [35]. The purified DO and DM exhibited the expected molecular weights by size exclusion chromatography without evidence of aggregation, as did the soluble DO–DM complex prepared by co-expression of sDO-Fc and sDM after removal of the Fc portions (Fig 1b). The inhibitory activities of DO-Fc, sDOv carrying the αP10aA mutation, and zippered szDOv were similar (Supplementary Fig 1). We measured the interaction of soluble DO and DM using biolayer interferometry. DM exhibits dose-dependent, saturable, tight-binding to szDO (Fig 1c). With increasing concentration, DO was able to completely inhibit DM catalysis of peptide binding (Fig 1d). We also evaluated DO's ability to inhibit DM-catalyzed peptide release from a pre-formed HLA-DR peptide complex. Dose-dependent inhibition of DM-mediated peptide release was observed (Fig 1e). Thus, DO can inhibit both the activity of DM in promoting peptide binding to MHCII molecules and its facilitation of peptide release from MHCII-peptide complexes.

Overview of DO–DM complex

To understand the mechanism by which DO inhibits DM, we determined the 3.2 Å crystal structure of the DO–DM complex, using DMα, DMβ, DOα-Fc, and DOβ-Fc subunits co-expressed in insect cells, with the Fc portions removed before crystallization (see Online Methods) and Table 1. Electron density for essentially all of DM and DO was observed except for a short section (DM β142-145). The two copies of the DO–DM complex present

in the crystallographic asymmetric unit showed little difference. DM binds to DO in a side-by-side arrangement, with three areas of contact involving each of the domains of the proteins (Fig 2a,b). In general, the structure of DM is essentially identical to those previously determined for DM alone [36–38], with one exception (see below). Strikingly, the structure of DO is distinct from DM and most similar to those previously determined for classical MHCII proteins and (Fig 2a, Supplementary Fig 2), but with alterations in the alpha subunit 3_{10} helix and adjacent extended strand region (described below).

In the DO–DM complex, the DM molecule rides on top of DO such that residues underneath its β-sheet platform contact residues above the end of the β-sheet platform of DO (Fig 2a,b). DM binds DO using the large concave surface underneath the end of the DM β-sheet platform and including edges of both membrane proximal immunoglobulin (Ig) domains (Fig 2b). Overall, DM and DO associate tightly with a complex three-part interface creating an extensive buried surface area of ~2800Å (Fig 2c, Supplementary Table 1). The interaction is distinct from that described for other MHCII proteins binding to partners such as αβTCR, CD4, bacterial superantigens, or another MHCII protein in the crystallographic dimer of MHCII molecules, or for classical and non-classical MHC I proteins binding to partners such as TfR, Fc, TCRγδ, or NK receptors.

Interactions between DO and DM

Interface I is the largest of the three main areas of contact between DM and DO, with about half of the total buried surface area (Fig 2, Supplementary Table 1). The major feature of this interface is the extended linker connecting DM's α1 and α2 domains (residues α91-100), a portion of which aligns with the last β strand (s4) of DO's β sheet platform (Fig 2d). The side chains of DM residues flanking the extended linker protrude into depressions in the DO surface (Fig 2e). DM αP95 fits into the cleft proximal to the α1 helix of DO, and DM αF100 fits in a large cavity formed between the upper peptide binding domain and the lower Ig domain of DO. In the center of this region, DM αR98 and DO αE40 make a salt bridge. In a reciprocal interaction, DO aromatic side chains αW43 and αF51, which flank the DO alpha subunit 3_{10} helix, fit into depressions in the DM surface (Fig 2e). Residues at the end of DMβ's β-strand platform and in the loop at the end of the DMβ1 helix participate in these interactions, including residues previously identified as the "acidic patch" (βD31 and E47) involved in the interaction with DR [39].

Interface II involves residues from the membrane-proximal Ig domains of the alpha subunits of DM and DO (Fig 2d). This predominantly hydrophobic interface contributes about one-third of the total surface buried area of the complex. Non-polar residues exposed on the surface of the last two β strands of the Ig domain (α173-194) of DM make a hydrophobic ridge against which lie three loops at the bottom of the DO Ig domain (α100-103, 129-134 and α151-153).

Interface III involves residues from the Ig domains of the beta subunits of DM and DO, and accounts for less than 20% of the total buried surface area (Fig 2d). Its major feature is a complimentary electrostatic interaction involving DM βR110 and DO βE187 residues. Structurally the arrangement in this interface is the reciprocal of interface 2, with residues from a DM loop connecting β strands in the Ig domain (β107-110) contacting residues from

DO (β96-100,180-181,183-187) exposed on the face of the Ig domain β strand. A small disordered region in DM's Ig domain (β142-145) is near the interface (Fig 2d dashed line, Supplementary Fig 3). Depending on its conformation, this segment might be able to mediate additional DO contacts (but see below).

DO adopts a MHCII fold with alpha subunit alterations

The DO–DM structure reveals an overall topology for DO highly similar to that of classical MHCII molecules such as HLA-DR1 (DR) (Fig 3a). For the alpha-subunit, DO superimposes well with both DR and DQ, with substantial Cα-backbone differences limited to the two structural elements that flank the 3_{10} helix, i.e. the last strand in the β-sheet platform (s4), and the extended region between the 3_{10} helix and the long α1-helical region. For the beta-subunit, DO superimposes well with DR and DQ throughout the sequence, with essentially no changes, except for a flexible loop (β106-11) in the Ig domain that adopts different conformations in the various MHCII structures determined to date [36,38].

The alpha subunit backbone differences have two consequences for the overall structure of the DO protein. The first is the zipping up of the β-sheet platform between strands s2 and s3 (Fig 3b). In DR, DQ and other MHCII proteins, the last two strands in the alpha subunit β-sheet platform veer away from the others (Fig 3b, right). In DO, strands s3 and s4 together shift ~2Å towards s2, forming a continuous H-bonding network between strands of the β-sheet platform (Fig3b, left). The structural change aligns DO strand s4 so that it can pair with DM (α96-99), which extends the continuous β-sheet platform by one strand.

The second consequence is a rearrangement of aromatic residues in the vicinity of the 3_{10} helix and adjacent extended strand region (Fig 3c). In DR and other MHCII proteins, this region interacts with bound peptide, with the extended strand participating in peptide main-chain interactions, and αW43, αF54, and βF89 lining the P1 peptide side-chain binding pocket (Fig 3c, right). In DO, the 3_{10} helix tilts (~12o) and the last turn partially unwinds. At the same time the first turn of the á1 helix also unwinds. As a consequence of the unwinding of both flanking helices, the extended strand is lengthened and undergoes a conformational change, displacing αF51 about 7Å and allowing the αW43 side chain to flip out (Fig 3c, left). In DR and other MHCII proteins, αW43 is tucked into the hydrophobic core lining the P1 pocket and unable to make contact with DM molecule. In DO αF54 has moved (5Å) into the region corresponding to the P1 pocket, displacing βF89, which flips out to the solvent previously occupied by αF51. Both αW43 and αF51 side chains thus become highly exposed on the outer face of DO and participate in key interactions with DM residues, forming the cornerstone of interface 1 (Fig 3c).

DO has a β-bulge the first β-strand of the alpha subunit that results in disruption of the H-bonding pattern at the center of the β-sheet platform (Fig 3d). For the human and murine MHCII proteins DR, DP and I-E, continuous H-bonding between the alpha subunit (s1) and beta subunit (s5) strands stabilizes the canonical anti-parallel β sheet conformation in this region. For the other MHCII proteins DQ and I-A, the β-bulge is present but allows the same number of H-bonds. For DO the inserted residue is proline present as the cis isomer, which orients the carbonyl O in a position that disrupts the H-bonding pattern and destabilizes interaction between the two chains. Substitution of αP10a by valine allows DO to egress the

ER in the absence of DM [35], presumably by restoring the canonical H-bonding pattern in the β-bulge region and stabilizing DO αβ chain pairing.

DM does not change conformation upon binding to DO

DM does not undergo a major conformational change upon binding to DO. Structural comparison with previously determined structures for HLA-DM and the murine homolog H2-M reveal Cα RMSD of only 0.7 $Å^2$ relative to DM in the DO–DM complex reported here, with essentially no overt conformational change in DM induced by DO binding, including the extended α1–α2 linker that aligns along the DO beta strand platform in the DO–DM complex (Supplementary Fig 3a–c). The only exception is the fourth β-strand (β131-149) in the membrane-proximal DM beta subunit IgG domain (Supplementary Fig 3d). In the free HLA-DM structure, this strand adopts a zig-zag conformation unusual among C-type IgG domains, with a large bulge (β131-136) interrupting the pattern of H-bonds to the adjacent strand (Supplementary Fig 3d). In the DO–DM structure, this strand adopts a different conformation, crossing over to the other sheet directly, as observed in the structure of the mouse DM homolog H-2DM. A small disordered region (β142-145) follows the crossover; despite the disorder this region clearly does not follow the same path as in the HLA-DM-only structure (Supplementary Fig 3e). Thus this region appears to be somewhat flexible. The region is nearby interface 3.

DM interacts similarly with MHCII and DO

The biological role of DM is to catalyze peptide exchange on MHCII proteins, and several studies have identified amino acid residues important to the interaction of DM with MHCII [6,39,40]. Because of the close structural similarity of MHCII and DO, we mapped these residues onto the structure of DO–DM complex (Figure 4). Strikingly, essentially all of the residues implicated in DM-MHCII interaction map to the interface between DM and DO, with most residues corresponding to direct DO–DM contacts. Each of the three interfaces is involved. Thus, the interaction of DM with MHCII, as identified in earlier mutagenesis studies, maps very closely to the sites of DO–DM interaction, as observed in the crystal structure.

To test the hypothesis that DM interacts similarly with MHCII and DO, we evaluated the effect of several mutations of DM, introduced at the putative MHCII interaction surface as defined by previous studies and also on a distal surface as a control (Fig 5a). For each mutant, we measured the relative DO–DM affinity using biolayer interferometry (Fig 5b), the effect on DM-catalyzed peptide exchange (Fig 5c), and for most mutations that preserve sufficient DM function, the effect on DO inhibition of DM (Fig 5d). The greatest effect was observed for αR98E,R194E (interface 1 and 2): this mutation reduced DO–DM binding affinity to 1/400 of the wild-type value and completely blocked DM-DR interaction as measured in a functional assay. Mutations βE8K and βE8A (periphery of interface 1), βL32N, which introduces an aberrant glycan at β32 (interface 1, acidic patch), and βR110S, which introduces an aberrant glycan at βN108, (interface 3) substantially reduced both DO binding and DR interaction. Control surface mutations βE39K,E183K,D188K and βE177N,I79T, which introduces an aberrant glycan at β177, exhibited comparable activity to wild type sDM in both assays. Together, these DM mutations have very similar effects on

interaction with DO and with MHCII, supporting a competitive mechanism for DO inhibition and a shared binding site for DO and MHCII.

One mutation had differential effects on interaction with DO and DR, a double alanine substitution of DM βH141 and S142, which flank the beginning of the flexibleβ2 region (β142-145, Supplementary Fig 3). This mutation reduced DO binding and was resistant to DO inhibition, but had essentially wild-type function in catalyzing peptide loading on DR (Fig 5b–d). To evaluate whether this phenomenon extended further into the disordered loop, we made additional mutants: two at position β144 (βA144E and βA144V) and also βH145N, which adds a glycan at this position. All three mutants had normal function in the assay of peptide-loading of DR (Fig 5c), and showed normal interaction with DO (Fig 5b, d). The basis for the differential role of DM βH141 and S142 in interaction with DO and DR currently is not clear.

Steady-state inhibition studies

The structural and the mutagenesis data presented above suggest that DO binds to the site used for catalysis of MHCII-peptide exchange, and thus might act as a competitive inhibitor. We used a steady-state enzyme kinetics approach to characterize the nature of DO inhibition of DM. The catalytic activity of DM in promoting both peptide binding to and release from MHCII molecules can be described using a Michaelis-Menten formalism [41] (Fig 6a). These kinetic parameters were altered in the presence of DO (Fig 6b). DO inhibition of DM action could be competitive, with DO binding to same site as the MHCII substrate and preventing its binding, or non-competitive, with DO binding at a different site as MHCII, inducing a conformational change that prevents catalysis while still allowing MHCII binding (Fig 6c). An uncompetitive mechanism, where DO would bind to a DM–MHCII complex, is unlikely since the DO–DM complex can form in the absence of MHCII.

A potential complication in analysis of enzyme inhibition is tight binding inhibition, which interferes with conventional Km Vm analysis [42]. Tight-binding inhibition can occur when the active enzyme concentration is approximately greater than or equal to the K_i^{app} [43] and can be identified by a linear dependence of IC_{50} on enzyme concentration when substrate is near the K_m and the IC_{50} is within 10-fold of the total enzyme concentration [42]. To test for tight-binding inhibition, the IC_{50} values of sDO(Ig) inhibition were determined at a range of sDM concentrations (Fig. 6d). The IC_{50} values increased linearly with sDM concentration, with K_i^{app} (0.29 ± 0.02 μM, see Methods) in the range of the sDM concentrations tested. This suggests that sDO exhibits tight-binding inhibition. Many tight-binding inhibitors are slow-onset. However, overnight preincubation of reaction components before peptide addition had no effect on the peptide binding rate (data not shown).

Competitive, noncompetitive and uncompetitive mechanisms in the presence of tight-binding inhibition can be differentiated by the Morrison analysis [42], in which the dependence of initial rate on substrate and inhibitor concentrations is described in terms of an apparent inhibition constant K_i^{app} that exhibits different concentration dependence for the different inhibition mechanisms (see Methods). Association data (Fig. 6e) were globally fit to the various inhibition model equations with statistical evaluation of model likelihood (see Methods). Relative to an uncompetitive model, the competitive model was preferred

($p<0.001$). For a noncompetitive model, α refined to a very large value (>1000), and the competitive model was still preferred with a probability ratio of 3:1. For a purely noncompetitive model ($\alpha=1$), the competitive model was preferred ($p<0.001$). We performed the same type of analysis using peptide dissociation data (Fig. 6f). These data had greater uncertainty, particularly at high pMHC concentration, limiting the confidence of model discrimination. However, the same pattern was observed, with the competitive model preferred over uncompetitive and non-competitive models, with α refining to a very high value. Thus, for both dissociation and association reactions, DO inhibition of DM catalysis was most consistent with a competitive inhibition model.

Discussion

The crystal structure, mutagnesis, and kinetic studies reported here provide a molecular mechanism for DO action: DO mimics an intermediate in the MHCII-peptide exchange reaction, and inhibits DM by binding tightly to the catalytic site and preventing MHCII access. This mechanism can help to discriminate models that previously have been postulated for DO function. In human B cells, approximately half of the total cellular DM is associated with DO [18,30], leading to suggestions that DO might qualitatively alter DM activity, for example modulating its peptide specificity in certain cells types or developmental stages [21,44]. However, the hypothetical DO–DM–MHCII ternary complex envisioned in these scenarios is not likely given the results presented here, as the DO–DM complex would be completely inactive in peptide loading / exchange reactions. A more attractive model has DO modulating the overall level of DM activity in a cell [45], changing the peptide repertoire by skewing towards a less constrained (i.e. less DM-resistant or less DM-edited) set of peptides. DO-deficient B cells are deficient in presentation of antigens brought into the cell via surface immunoglobulin but not fluid-phase endocytosis [28], suggesting a role for DO in focusing DM's attention on antigen presentation pathways most relevant for B cell function [21]. A potential mechanism based on differential inhibition of DM by DO in intracellular compartments with different pH [28] would appear to be ruled out by findings that DO can inhibit DM throughout the entire pH range in which DM is active [21,31]. Thus, how DO regulates flux through the various intracellular antigen presentation pathways has not been clear. The results presented here together with previous studies of the intracellular localization of DO might provide a clue. Using immunoelectron microscopy, van Lith et al. observed DO at the limiting perimeter membrane but not the internal membranes of the multivesicular bodies characteristic of MHCII-containing compartments (MIIC) in antigen presenting cells [46]. Subsequent FRET studies revealed that the interaction of DM with MHCII was spatially regulated, with DM able to interact with MHCII in only internal vesicles but not the limiting membrane [44]. Inhibition of DM by DO present only in the limiting membrane would explain this pattern. Recently, Xiu et al observed in transfected cells that DO impaired the incorporation of DM into exosomes using di-leucine motif in the HLA-DOβ cytoplasmic tail [47]. Since exosomes are believed to derive from internal vesicles released from multivesicular bodies by fusion with the plasma membrane, the same mechanism would be likely to retain DO–DM complexes in the limiting membrane. Thus, DO would be expected to inhibit DM throughout the endocytic pathway except for the internal compartments of the multivesicular bodies. These

compartments would provide a DO-free zone for the preferential utilization of receptor-internalized antigens. Consistent with this idea, persisting antigens internalized into non-terminal late endosomes via B-cell receptor uptake exhibit a higher degree of colocalization with DM as compared to DO [48].

The structure of HLA-DO provides insight into the nature of αβ subunit association for both classical and non-classical MHCII proteins and helps to explain the effects on DO stability and trafficking observed for substitution at αP10a. The H-bonding network in the intersubunit region at the center of the beta sheet platform below the helices appears to play an important role in the stability and assembly of classical MHC II αβ dimer [49]. In general, studies have shown that MHCII proteins with mismatched subunits are retained in the ER [50]. Substitution of proline α10a by valine or alanine allows DO to egress the ER in the absence of DM. The requirement of DM for DO to egress the ER was interpreted as a structural defect that was compensated by DM [35]. We suggest that replacement of αP10a, or of DOα[1–18] with DRα[1–18] [35], restores the canonical continuous H-bonding in this region and stabilizes DO αβ chain pairing. The interface with DM involves large portions of the lateral surface of both DO α and β subunits, with interactions distributed broadly between the β–sheet platform and Ig domains. The chaperone-like function of DM in regulating DO transport is likely to result from cooperative interactions between these sites leading to stabilization of DO αβ pairing. The chaperone-like effect of DM on stabilizing classical MHCII proteins in the absence of peptide [11,12,51] might work by a similar mechanism.

Despite the structural similarity of DO to classical MHCII proteins and strong conservation of the interface residues, DM binds tightly and essentially irreversibly to DO but only transiently to MHCII. The structure reported here provides insight into how DO has adapted the generic MHCII structure for irreversible binding and functional inhibition of DM. First, the Pα10a beta bulge mentioned above disrupts DO α-β chain pairing, and enforces a requirement for DM binding [35]. In the absence of peptide, MHCII proteins also are relatively unstable unless chaperoned by DM [11,12]. This is particularly true for variants such as HLA-DQ and I-A that share the beta bulge at residue α10a. Second, DO appears not to bind peptide or other ligands, despite having a membrane-distal groove sharing many characteristics of the classical MHCII peptide binding groove. For MHCII proteins, release from DM is thought to result from conformational changes induced by peptide binding[6,9,52]. It is possible that DO remains locked in a DM-binding conformation because it cannot bind peptide and access peptide-induced conformational changes. In classical MHCII-peptide complexes, the key DM-interacting residues W43α and F51α are largely inaccessible, but conformational changes around the 3_{10} helix and P1 pocket, as observed in the structure of DR1 mutant αF54C with increased DM interaction [9], and in a molecular dynamics simulation of peptide-free MHCII [53], provide a framework for understanding how MHCII conformational changes can expose these residues and couple DM binding with MHC II peptide release. However, it is important to note that while W43α and F51α are conserved in DO and play prominent roles in the DM-DO interface, the three-dimensional structure of free DO is not known, and so further studies will be required to determine whether the tighter DM binding of DO as compared to MHCII is due to differences in the static structures or to structural changes induced in DO upon binding DM.

Online Methods

Protein expression

sDO-Fc [28], sDM [55], and sDR [2] constructs were described previously. For szDOv, the point mutation αP10aA was introduced into the alpha subunit extracellular domain, and $(GGGS)_2$ linker, C3 protease recognition site, acid leucine zipper sequence, and His_6 purification tag were added. In the original characterization of this mutation [35] the αP10a position is labeled αP11, but here we use the canonical MHCII numbering system developed for I-A(b) in which the position is labeled αP10a to maintain concordance with the numbering of the remainder of the MHCII alpha subunit. The szDO beta subunit was constructed similarly but with basic leucine zipper sequence and M2 FLAG epitope tag. sDOFc, szDOv, sDM, sDR1, and sDR4 were expressed as soluble proteins in stably transfected Schneider-2 *Drosophila melanogaster* cells. Proteins were collected from concentrated and buffer-exchanged conditioned medium 5–7 days post induction (1 mM $CuSO_4$) by affinity chromatography: protein A-agarose (Repligen) affinity with acid elution for sDOFc, M2-agarose (Sigma) immunoaffinity with FLAG peptide elution for sDM, sequential protein A affinity and M2-agarose capture for coexpressed sDM–sDOFc, NiNTA-agarose affinity with histidine elution or M2-agarose capture for szDOv, and LB3.1 immunoaffinity [56] with alkali elution for DR. Protein containing fractions were pooled, concentrated by ultrafiltration (Amicon 10,000 MWCO), further purified and separated from protein aggregates by size exclusion chromatography (SEC) over Superdex 200 (GE Healthcare) in phosphate buffered saline (PBS), and stored at 4°C before use. Before SEC, Fc regions were removed from sDOFc and sDM–sDOFc using activated papain conjugated to agarose (Sigma) at an approximate DO:papain ration of 0.5:1 in 100 mM citrate buffer (pH 5.9), 50 mM NaCl and 1 mM EDTA at 37°C for 3 hrs and quenched with 10 μM E-64, or zippers were removed from szDOv using HRV C3 protease (Novagen). In some experiments sDR1 was prepared by expression in *E. coli* inclusion bodies and folded *in vitro*, as described [56].

Protein-protein interaction

In the Octet QK biosensor (Fortebio, Menlo Park, CA), binding of an analyte in solution to a ligand immobilized on the sensor tip changes the interference pattern of white light reflected from the sensor surface relative to a reference surface and is measured as the wavelength (nm) shift. To achieve homogenous immobilization of sDM or szDOv to streptavidin-coated biosensor tips (Fortebio), we engineered the sDM alpha chain or the szDOv beta chain with a C-terminal Avitag, such that recombinant proteins can be specifically biotinylated using BirA ligase. For assays, streptavidin-coated biosensor tips were hydrated for 30–60 min using PBST (phosphate-buffered saline with 0.1 mg/ml BSA, 0.002% Tween 20, pH 7.2) and loaded with biotinylated ligands (e.g., bio-szDOv) in PBST at a concentration of 1.6 μg/ml, briefly washed, and then incubated with various concentrations of analytes (e.g, wt or mutant sDM) in PBST to allow association. Assays were performed at 25°C in black 96-well plates (E&K Scientific) under orbital shaking conditions (1000 rpm). We were not able to identify suitable regeneration conditions and so each biosensor tip was used once. Assays were repeated at least 3 times. No binding of a control protein (mouse immunoglobulin) to szDO was observed (not shown). Immobilization of bio-sDM followed by the measurement of association of szDOv was performed similarly. Data were analyzed using Origin software

(Fortebio). The wavelength shift, representing the amount of sDM-szDOv complexes formed on the sensor surface at each analyte concentration, was plotted against time and fit to a single exponential association curve:

$$Y = Yo + Y_{max}\,(1 - e^{-kobs^{*}t})$$

where Y_0 is the initial wavelength shift, Y is the observed wavelength shift at time t, Y_{max} is the maximum wavelength shift at a given analyte concentration, and k_{obs} is the observed first order rate constant. Fitted values for Y_{max} at each analyte concentration were then fit to a single site binding model:

$$Y_{max} = S^{*}[C]/(K_D{}^{\mathrm{app}} + [C])$$

Where S is the wavelength shift representing saturation binding of the analyte to the ligand immobilized on the biosensor surface, [C] is the analyte concentration and K_D^{app} is the apparent equilibrium constant.

Real-time kinetic measurements of peptide-MHCII association and dissociation

Peptides HA (Ac-PRFVKQNTLRLAT) derived from influenza hemagglutinin and CLIP (Ac-VSKMRMATPLLMQ) derived from the MHCII-associated invariant chain each have a single amino group (Lys Nε) that was labeled with 7-amino-4-methylcoumarin-3-acetic acid succinimide ester (AMCA-NHS, Pierce) for FRET measurements [57] or with Alexa-488 carboxylic acid, 2,3,5,6-tetrafluorophenyl ester (Molecular Probes) for fluorescence polarization studies [53]. Labeled peptides were isolated by reverse-phase chromatography and verified by mass spectrometry. For FRET measurement of peptide association rates, AMCA-HA peptide binding to sDR1 was monitored using the FRET from tryptophan residues in sDR1 to AMCA [57], at various concentrations of sDR1, peptide, sDM, and szDOv, szDO, sDOFc, sDM–sDOFc, or sDM–sDO, as indicated, All experiments were performed in 20 mM citrate buffer, pH 5, 150 mM NaCl, 0.01% Tween-20, 0.02% sodium azide at 37°C. The fraction of “peptide-receptive” sDR1 in similar preparations is 2–10% [57]. The effect of peptide dissociation during the assay is negligible, because the $t_{1/2}$ of HA peptide/sDR1 is >100h under these conditions [58]. FRET was measured using λ_{ex} 280 nm and λ_{em} 460 nm in a fluorescence plate reader (Polarstar Optima, BMG Labtech), with purified AMCA-HA peptide and purified sDR1/AMCA-HA as standards. For polarization measurements of peptide dissociation rates, sDR1/Alexa-CLIP complexes were prepared by extended incubation of sDR1 and excess peptide at 37°C in 0.1 M Na citrate, pH 5.5, 0.05 M NaCl, 0.1 mg/ml PMSF, 37 μg/ml iodoacetamide, 5 mM EDTA, 0.02 % NaN_3, 0.05% octyl-β-glucoside followed by isolation using SEC (Superdex S200) in PBS. Fluorescence polarization was measured using λ_{ex}=485 nm and λ_{em}=520 nm in a fluorescence plate reader (Victor-X, Perkin-Elmer) and expressed as millipolarization units (mP). Purified Alexa-CLIP peptide (~70 mP) and sDR1/Alexa-CLIP (~350 mP) were used as standards. For IC_{50} measurement, the fraction active was determined by dividing the initial rate of peptide association in the presence of sDM and sDO by the uninhibited rate determined in the presence of sDM, but not sDO. Fraction active values were plotted versus log[DO] and fit to

a single site inhibition model to generate IC_{50} values. sDO–sDM or szDOv incubated with peptide without sDR1 showed no significant change in FRET or mP change over time, and control proteins bovine serum albumin, mouse immunoglobulin G, and chicken egg white lysozyme showed no significant activity in facilitating peptide binding to sDR1 or in inhibiting DM-mediated peptide exchange (data not shown). See Supplementary note for methods used in enzyme inhibition studies.

Endpoint peptide loading assays

sDR4-CLIP (10 nM) and biotinylated HA peptide (bio-PKYVKQNTLKLAT, 10 μM) were incubated in the presence or absence of various concentrations of wild type or mutant sDM in the reaction buffer (50 mM sodium acetate buffer, pH 5.0, 150 mM NaCl, 1% (w/v) BSA, 0.5% (v/v) NP40, 0.05% (w/v) NaN3, 1X EDTA-free Complete protease inhibitor (Santa Cruz Biotechnology, Inc.)) at 37°C for 2 h. After incubation, reactions were neutralized with two volumes of ice-cold neutralization buffer (50 mM Tris–Cl, pH 8.2, 150 mM NaCl, 1% (w/v) BSA, 0.5% (v/v) NP40, 0.05% (w/v) NaN_3) for downstream capturing and detection of HA-loaded sDR4 using a time-resolved-fluorescence-based ELISA method [55]. For DO inhibition studies, various concentrations of szDOv were also introduced into the reaction before incubation. Samples were all prepared and mixed on ice in order to maintain the stability of proteins and to minimize the variation of incubation time at higher temperature.

Structure determination

Crystals of the sDO–sDM complex crystals grew from 100 mM Na acetate pH 4.6 and 8% PEG 4K in hanging drops at room temperature. A single crystal (500 × 100 × 10 μm) was transferred to cryoprotectant containing 20% PEG 4K and 20% glycerol, rapidly cooled in liquid nitrogen, and used for data collection at 100K at National Synchrotron Light Source (NSLS) beamline x25 (wavelength) at Brookhaven National Laboratory. Data collection and refinement statistics are shown in Table 1, with R_{pim} calculated according to reference [54]. X-ray images were processed using HKL2000 [59]. Phaser [60] molecular replacement using 2BC4 (DM) and 1KLU (DR1) as search models for DM and DO, respectively, identified a single strong solution (Z score = 28) representing two DO–DM dimers in the asymmetric unit, with weaker solutions corresponding to alignment of DM with DO and vice versa. CNS composite omit [61] and resolve prime-and-switch [62] maps revealed clear density for 80% of DM and 40% of DO residues (Supplementary Fig 4a). SHELXL [63] was used to generate a test set (R_{free}) comprising 5% of the reflections selected in thin resolution shells and strict 2-fold non-crystallographic symmetry restraints were imposed for cycles of crystallographic refinement in Phenix [64]. Initial electron density maps were improved by iterative averaging of non-crystallographic related domains, manual model building using coot [65], and automated refinement cycles, which included position and atomic B factor refinement, Ramachandran restraints and rigid body refinement. Data collection statistics in the highest resolution shell are poor, but inclusion of these data significantly reduced the R_{free} values in the adjacent resolution shell [66]. In the final model 94.4% of the residues were in favored regions of Ramachandran plot with 5.6% in allowed regions. RMSD between non-crystallographically related molecules was 0.43 Å for DM and 0.23 Å for DO. Regions of MHCII-DO conformational difference were not near crystal contacts. No extra electron density was observed was observed in the DO region corresponding to the MHCII peptide

binding groove (Supplementary Fig 4b). Crystallographic data and atomic coordinates will be available from the Protein Data Bank with accession code 3USA.

Supplementary Material

Refer to Web version on PubMed Central for supplementary material.

Acknowledgments

We thank Lars Karlsson for S2 cells expressing DM and DO-Fc, Jacques Thibodeau (Université de Montréal, Canada) for pRmHa3 encoding sDOα and sDOβ cDNAa, Loretta Lee and Liying Lu for assistance with insect cell culture and protein purification, Howard Robinson and Annie Heroux for assistance with crystallographic data collection, and Efstratios Stratikos for helpful comments. Data for this study were measured at beamlines X25, and X29 of the National Synchrotron Light Source, supported by the Offices of Biological and Environmental Research and of Basic Energy Sciences of the US Department of Energy, and from the National Center for Research Resources of the National Institutes of Health. This work was supported by National Institutes of Health grants AI-38996 (LJS), AI-48833 (LJS), T32 AI07349 (SEM), F32 AI072984 (SEM), AI-095813 (EDM), AI-075253 (EDM) and Stanford NIH/NCRR CTSA, UL1 RR025744, together with the Lucile Packard Foundation for Children's Health (EDM).

References

1. Denzin LK, Cresswell P. HLA-DM induces CLIP dissociation from MHC class II alpha beta dimers and facilitates peptide loading. Cell. 1995; 82:155–65. [PubMed: 7606781]
2. Sloan VS, et al. Mediation by HLA-DM of dissociation of peptides from HLA-DR. Nature. 1995; 375:802–6. [PubMed: 7596415]
3. Ghosh P, Amaya M, Mellins E, Wiley DC. The structure of an intermediate in class II MHC maturation: CLIP bound to HLA-DR3. Nature. 1995; 378:457–62. [PubMed: 7477400]
4. Morris P, et al. An essential role for HLA-DM in antigen presentation by class II major histocompatibility molecules. Nature. 1994; 368:551–4. [PubMed: 8139689]
5. Riberdy JM, Newcomb JR, Surman MJ, Barbosa JA, Cresswell P. HLA-DR molecules from an antigen-processing mutant cell line are associated with invariant chain peptides. Nature. 1992; 360:474–7. [PubMed: 1448172]
6. Anders AK, et al. HLA-DM captures partially empty HLA-DR molecules for catalyzed removal of peptide. Nat Immunol. 2010
7. Ferrante A, Gorski J. Cutting edge: HLA-DM-mediated peptide exchange functions normally on MHC class II-peptide complexes that have been weakened by elimination of a conserved hydrogen bond. J Immunol. 2009; 184:1153–8. [PubMed: 20038641]
8. Narayan K, et al. HLA-DM targets the hydrogen bond between the histidine at position beta81 and peptide to dissociate HLA-DR-peptide complexes. Nat Immunol. 2007; 8:92–100. [PubMed: 17143275]
9. Painter C, et al. Conformational lability in the class II MHC 310 helix and adjacent extended strand dictate HLA-DM susceptibility and peptide exchange. Proc Natl Acad Sci U S A. 2011 in press.
10. Zhou Z, Callaway KA, Weber DA, Jensen PE. Cutting edge: HLA-DM functions through a mechanism that does not require specific conserved hydrogen bonds in class II MHC-peptide complexes. J Immunol. 2009; 183:4187–91. [PubMed: 19767569]
11. Denzin LK, Hammond C, Cresswell P. HLA-DM interactions with intermediates in HLA-DR maturation and a role for HLA-DM in stabilizing empty HLA-DR molecules. J Exp Med. 1996; 184:2153–65. [PubMed: 8976171]
12. Kropshofer H, Arndt SO, Moldenhauer G, Hammerling GJ, Vogt AB. HLA-DM acts as a molecular chaperone and rescues empty HLA-DR molecules at lysosomal pH. Immunity. 1997; 6:293–302. [PubMed: 9075930]
13. Weber DA, Evavold BD, Jensen PE. Enhanced dissociation of HLA-DR-bound peptides in the presence of HLA-DM. Science. 1996; 274:618–20. [PubMed: 8849454]

14. Tonnelle C, DeMars R, Long EO. DO beta: a new beta chain gene in HLA-D with a distinct regulation of expression. The EMBO journal. 1985; 4:2839–47. [PubMed: 2998758]
15. Douek DC, Altmann DM. T-cell apoptosis and differential human leucocyte antigen class II expression in human thymus. Immunology. 2000; 99:249–56. [PubMed: 10692044]
16. Hornell TM, et al. Human dendritic cell expression of HLA-DO is subset specific and regulated by maturation. J Immunol. 2006; 176:3536–47. [PubMed: 16517722]
17. Karlsson L, Surh CD, Sprent J, Peterson PA. A novel class II MHC molecule with unusual tissue distribution. Nature. 1991; 351:485–8. [PubMed: 1675431]
18. Chen X, et al. Regulated expression of human histocompatibility leukocyte antigen (HLA)-DO during antigen-dependent and antigen-independent phases of B cell development. J Exp Med. 2002; 195:1053–62. [PubMed: 11956296]
19. Glazier KS, et al. Germinal center B cells regulate their capability to present antigen by modulation of HLA-DO. J Exp Med. 2002; 195:1063–9. [PubMed: 11956297]
20. Chen X, Reed-Loisel LM, Karlsson L, Jensen PE. H2-O expression in primary dendritic cells. Journal of immunology. 2006; 176:3548–56.
21. Denzin LK, Fallas JL, Prendes M, Yi W. Right place, right time, right peptide: DO keeps DM focused. Immunol Rev. 2005; 207:279–92. [PubMed: 16181343]
22. Jensen PE. Antigen processing: HLA-DO--a hitchhiking inhibitor of HLA-DM. Curr Biol. 1998; 8:R128–31. [PubMed: 9501976]
23. Yi W, et al. Targeted regulation of self-peptide presentation prevents type I diabetes in mice without disrupting general immunocompetence. J Clin Invest. 2010; 120:1324–36. [PubMed: 20200448]
24. Perraudeau M, et al. Altered major histocompatibility complex class II peptide loading in H2-O-deficient mice. Eur J Immunol. 2000; 30:2871–80. [PubMed: 11069069]
25. van Ham SM, et al. HLA-DO is a negative modulator of HLA-DM-mediated MHC class II peptide loading. Curr Biol. 1997; 7:950–7. [PubMed: 9382849]
26. Alfonso C, et al. Analysis of H2-O influence on antigen presentation by B cells. J Immunol. 2003; 171:2331–7. [PubMed: 12928379]
27. Alfonso C, Williams GS, Karlsson L. H2-O influence on antigen presentation in H2-E-expressing mice. Eur J Immunol. 2003; 33:2014–21. [PubMed: 12884868]
28. Liljedahl M, et al. Altered antigen presentation in mice lacking H2-O. Immunity. 1998; 8:233–43. [PubMed: 9492004]
29. Denzin LK, Sant'Angelo DB, Hammond C, Surman MJ, Cresswell P. Negative regulation by HLA-DO of MHC class II-restricted antigen processing. Science. 1997; 278:106–9. [PubMed: 9311912]
30. Liljedahl M, et al. HLA-DO is a lysosomal resident which requires association with HLA-DM for efficient intracellular transport. EMBO J. 1996; 15:4817–24. [PubMed: 8890155]
31. Yoon T, et al. Mapping the DO/DM complex by FRET and mutagenesis. Proc Natl Acad Sci U S A. 2012; 109:11276–81. [PubMed: 22733780]
32. Fallas JL, et al. Ectopic expression of HLA-DO in mouse dendritic cells diminishes MHC class II antigen presentation. J Immunol. 2004; 173:1549–60. [PubMed: 15265882]
33. Thibodeau J, et al. Conserved structural features between HLA-DO beta and -DR beta. Mol Immunol. 1998; 35:885–93. [PubMed: 9839557]
34. Kropshofer H, et al. A role for HLA-DO as a co-chaperone of HLA-DM in peptide loading of MHC class II molecules. EMBO J. 1998; 17:2971–81. [PubMed: 9606180]
35. Deshaies F, et al. A point mutation in the groove of HLA-DO allows egress from the endoplasmic reticulum independent of HLA-DM. Proc Natl Acad Sci U S A. 2005; 102:6443–8. [PubMed: 15849268]
36. Fremont DH, Crawford F, Marrack P, Hendrickson WA, Kappler J. Crystal structure of mouse H2-M. Immunity. 1998; 9:385–93. [PubMed: 9768758]
37. Mosyak L, Zaller DM, Wiley DC. The structure of HLA-DM, the peptide exchange catalyst that loads antigen onto class II MHC molecules during antigen presentation. Immunity. 1998; 9:377–83. [PubMed: 9768757]

38. Nicholson MJ, et al. Small molecules that enhance the catalytic efficiency of HLA-DM. J Immunol. 2006; 176:4208–20. [PubMed: 16547258]
39. Pashine A, et al. Interaction of HLA-DR with an acidic face of HLA-DM disrupts sequence-dependent interactions with peptides. Immunity. 2003; 19:183–92. [PubMed: 12932352]
40. Doebele RC, Busch R, Scott HM, Pashine A, Mellins ED. Determination of the HLA-DM interaction site on HLA-DR molecules. Immunity. 2000; 13:517–27. [PubMed: 11070170]
41. Vogt AB, Kropshofer H, Moldenhauer G, Hammerling GJ. Kinetic analysis of peptide loading onto HLA-DR molecules mediated by HLA-DM. Proc Natl Acad Sci U S A. 1996; 93:9724–9. [PubMed: 8790398]
42. Copeland, R. A practical introduction to structure, mechanism, and data analysis. 2. Vol. Chapter 9. Wiley-VCH; 2000. Enzymes.
43. Williams JW, Morrison JF. The kinetics of reversible tight-binding inhibition. Methods Enzymol. 1979; 63:437–67. [PubMed: 502865]
44. Zwart W, et al. Spatial separation of HLA-DM/HLA-DR interactions within MIIC and phagosome-induced immune escape. Immunity. 2005; 22:221–33. [PubMed: 15723810]
45. van Ham M, et al. Modulation of the major histocompatibility complex class II-associated peptide repertoire by human histocompatibility leukocyte antigen (HLA)-DO. J Exp Med. 2000; 191:1127–36. [PubMed: 10748231]
46. van Lith M, et al. Regulation of MHC class II antigen presentation by sorting of recycling HLA-DM/DO and class II within the multivesicular body. J Immunol. 2001; 167:884–92. [PubMed: 11441095]
47. Xiu F, et al. Cutting edge: HLA-DO impairs the incorporation of HLA-DM into exosomes. Journal of immunology. 2011; 187:1547–51.
48. Gondre-Lewis TA, Moquin AE, Drake JR. Prolonged antigen persistence within nonterminal late endocytic compartments of antigen-specific B lymphocytes. J Immunol. 2001; 166:6657–64. [PubMed: 11359820]
49. Sant AJ, Braunstein NS, Germain RN. Predominant role of amino-terminal sequences in dictating efficiency of class II major histocompatibility complex alpha beta dimer expression. Proc Natl Acad Sci U S A. 1987; 84:8065–9. [PubMed: 3120183]
50. Sant AJ, Hendrix LR, Coligan JE, Maloy WL, Germain RN. Defective intracellular transport as a common mechanism limiting expression of inappropriately paired class II major histocompatibility complex alpha/beta chains. J Exp Med. 1991; 174:799–808. [PubMed: 1919435]
51. Rinderknecht CH, et al. DM influences the abundance of major histocompatibility complex class II alleles with low affinity for class II-associated invariant chain peptides via multiple mechanisms. Immunology. 2010; 131:18–32. [PubMed: 20408893]
52. Ferrante A, Anderson MW, Klug CS, Gorski J. HLA-DM mediates epitope selection by a “compare-exchange” mechanism when a potential peptide pool is available. PLoS One. 2008; 3:e3722. [PubMed: 19005572]
53. Painter CA, Cruz A, Lopez GE, Stern LJ, Zavala-Ruiz Z. Model for the peptide-free conformation of class II MHC proteins. PLoS One. 2008; 3:e2403. [PubMed: 18545669]
54. Weiss MS. Global indicators of X-ray data quality. J Appl Cryst. 2001; 34:130–135.
55. Busch R, Doebele RC, von Scheven E, Fahrni J, Mellins ED. Aberrant intermolecular disulfide bonding in a mutant HLA-DM molecule: implications for assembly, maturation, and function. J Immunol. 1998; 160:734–43. [PubMed: 9551909]
56. Frayser M, Sato AK, Xu L, Stern LJ. Empty and peptide-loaded class II major histocompatibility complex proteins produced by expression in Escherichia coli and folding in vitro. Protein Expr Purif. 1999; 15:105–14. [PubMed: 10024477]
57. Joshi RV, Zarutskie JA, Stern LJ. A three-step kinetic mechanism for peptide binding to MHC class II proteins. Biochemistry. 2000; 39:3751–62. [PubMed: 10736175]
58. Zarutskie JA, et al. The kinetic basis of peptide exchange catalysis by HLA-DM. Proc Natl Acad Sci U S A. 2001; 98:12450–5. [PubMed: 11606721]
59. Otwinoski Z, Minor W. Processing of X-ray Diffraction Data Collected in Oscillation Mode. Methods in Enzymology. 1997; 276:307–326.

60. McCoy AJ, et al. Phaser crystallographic software. J Appl Crystallogr. 2007; 40:658–674. [PubMed: 19461840]

61. Brunger AT, et al. Crystallography & NMR system: A new software suite for macromolecular structure determination. Acta Crystallogr D Biol Crystallogr. 1998; 54:905–21. [PubMed: 9757107]

62. Terwilliger TC. Maximum-likelihood density modification. Acta Crystallogr D Biol Crystallogr. 2000; 56:965–72. [PubMed: 10944333]

63. Sheldrick GM, Schneider TR. SHELXL: high-resolution refinement. Methods Enzymol. 1997; 277:319–43. [PubMed: 18488315]

64. Adams PD, et al. PHENIX: a comprehensive Python-based system for macromolecular structure solution. Acta Crystallogr D Biol Crystallogr. 2010; 66:213–21. [PubMed: 20124702]

65. Emsley P, Cowtan K. Coot: model-building tools for molecular graphics. Acta Crystallogr D Biol Crystallogr. 2004; 60:2126–32. [PubMed: 15572765]

66. Karplus PA, Diederichs K. Linking crystallographic model and data quality. Science. 2012; 336:1030–3. [PubMed: 22628654]

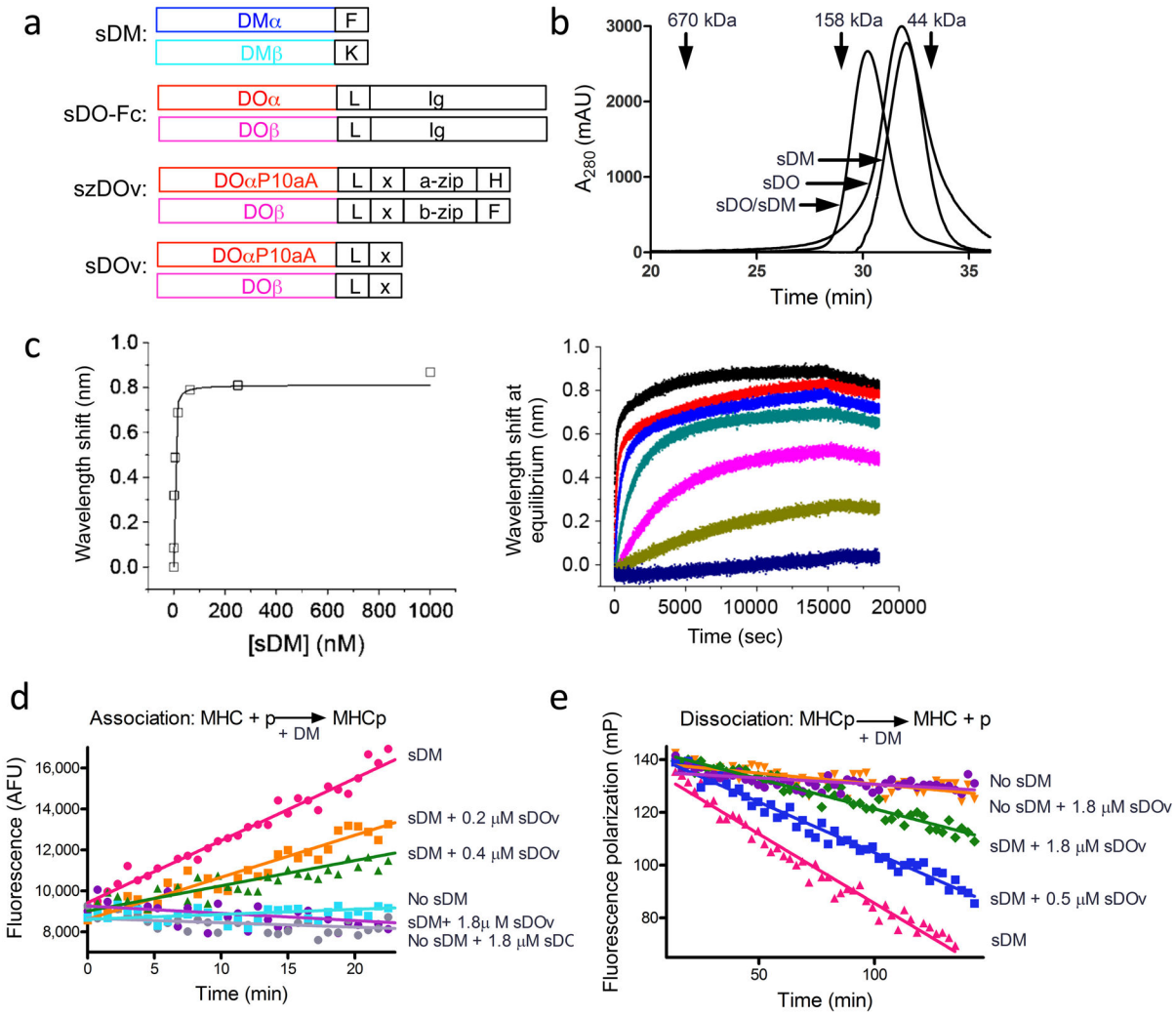

Figure 1. HLA-DO binds to HLA-DM and inhibits DM-catalyzed peptide binding and release

(A) Schematic representation of DM and modifications introduced into DO α and β chains to allow production of stable recombinant protein: Fc domains (sDO-Fc), αP10aA mutation and Leu zippers (szDOv) and αP10aA mutation only (sDOv), F, FLAG tag, H, hexahistidine tag, K, KT3 epitope tag, L, linker, Ig, immunoglobulin CH3 domain, x, C3 protease cleavage site, a-zip and b-zip, acid and basic leucine zipper dimerization sequences. (B) Size exclusion chromatography over S200. Retention times of molecular weight markers are indicated. (C) *Left*, concentration dependent binding of sDM to immobilized biotinylated sDO (top trace to bottom, 4-fold dilutions starting from 1μM), *Right*, equilibrium wavelength shift values plotted against [sDM] and fit to a single-site binding model. (D) sDM-catalyzed peptide binding to sDR in the presence of various concentration of szDOv as indicated, 0.3μM sDM, 0.08μM AMCA-HA and 0.5μM sDR1. 'No sDM + 1.8μM sDOv' and 'no sDM' indicate uncatalyzed binding of peptide to sDR with and without sDOv, respectively. (E) sDM-catalyzed peptide dissociation from the sDR/CLIP-Alexa complex (25 nM) in the presence of various concentrations of sDOv as indicated and 0.025μM sDR/

CLIP-Alexa complex, 12.5μM unlabeled HA peptide and 0.1μM sDM. Data are representative of at least 3 experiments.

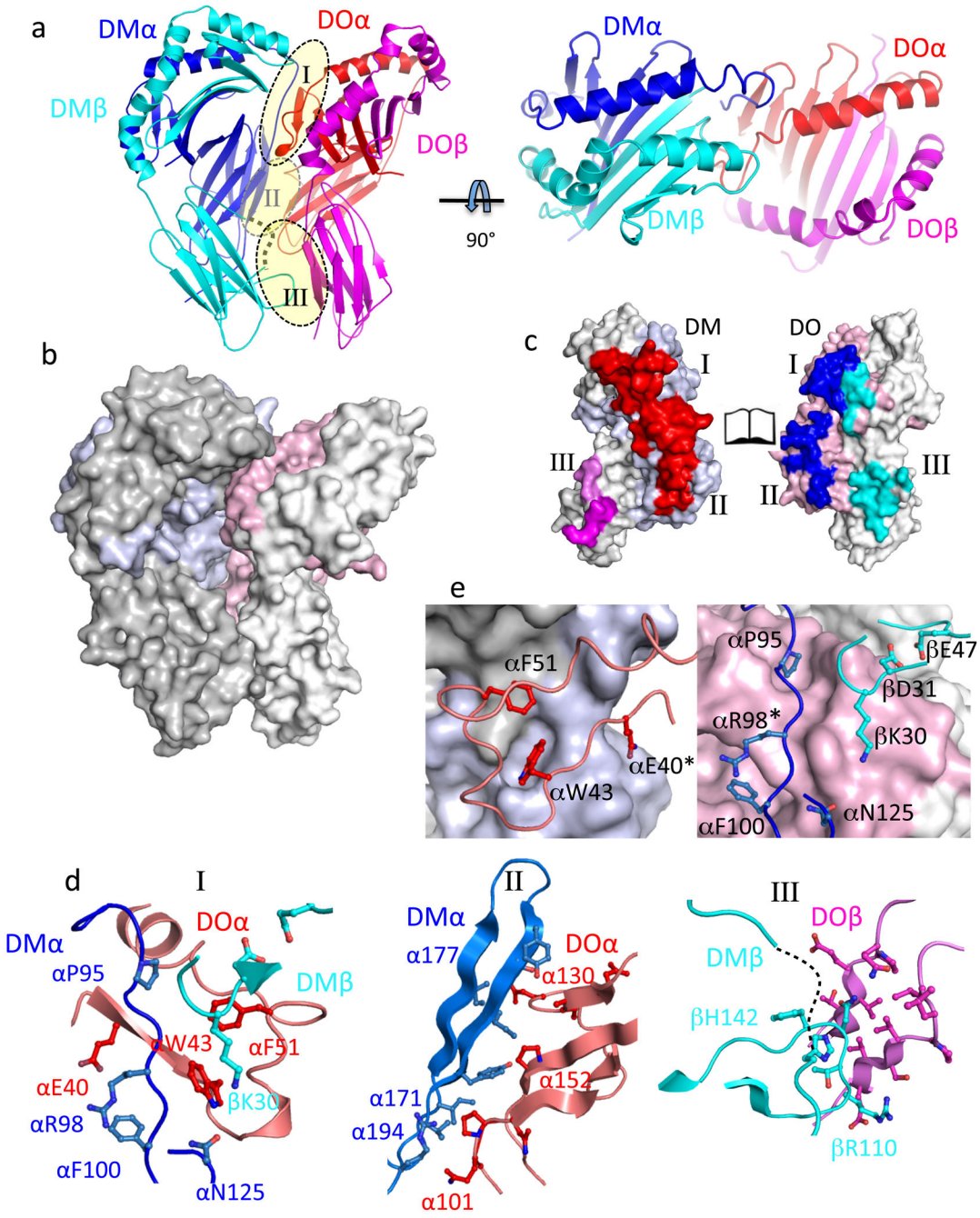

Figure 2. Structure of the DM – DO complex

(A) HLA-DM (α, blue; β,cyan) in complex with DO (α, red; β, magenta). The three major DO–DM interfaces are highlighted. (B) Surface representation of view in panel A, colored similarly but with DMα gray and DOβ white. (C) Surface representation of DO–DM complex opened up like a book, with contact areas colored according to the subunit contacted. For DM (left), red and magenta represent the interface with DO α and β residues, respectively. For DO (right), blue and cyan represent the interface with DO α and β residues, respectively. (D) DM–DO interfaces. In interface I, residues from DMα linking the upper

and lower domains (shown in blue) and from exposed loops at the end of the beta-sheet platform from DMβ (cyan) contact residues from the 3_{10} helix and adjacent strands of DOα (red). In interface II, residues at the loops of the Ig domain of DOα pack against the side of DMα Ig-domain β-sheet. In interface II, residues at the loops of the Ig domain of DMβ packs against the side of DOα Ig-domain β-sheet. A disordered regions in DMβ is shown as a dashed line. (E) Surface view of interface 1, opened up as in panel C. DM surface (left) shows small pockets that accommodate side chains of DO. DO surface (right) buries DM residues αP95 and αF100.

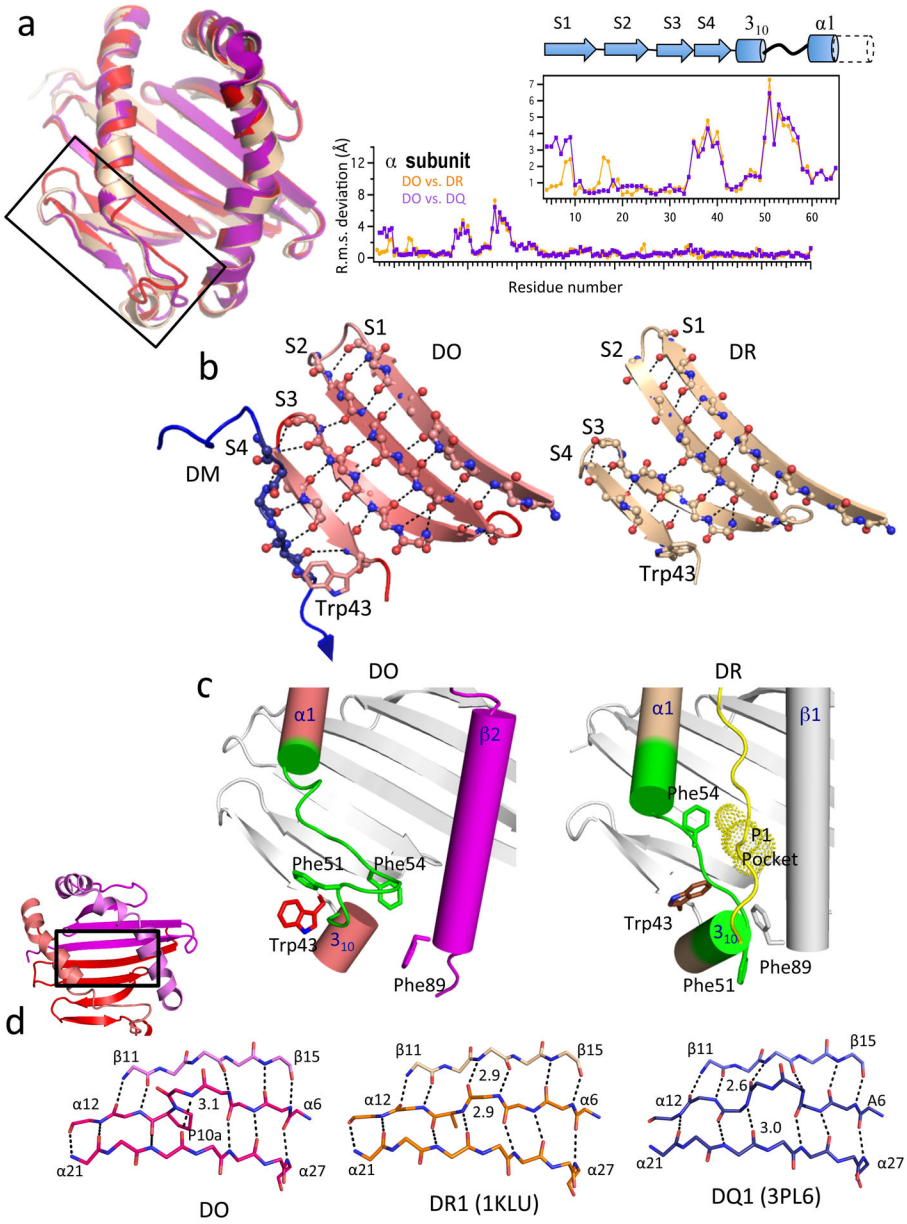

Figure 3. The HLA-DO structure is very similar to conventional MHCII proteins, but with alterations in the alpha subunit 3_{10} helix and adjacent extended strand

(A) *Left*, Overlay of upper domains of HLA-DO (colored red and magenta) and conventional MHCII (tan). Region of conformational alteration is boxed. *Right*, RMSD between DO and DR1 (1KLU, yellow) or DQ1 (3PL6, purple) alpha subunits, showing large changes in regions flanking the 3_{10} helix. (B) Alteration in the beta-sheet platform strand pairing. In DR, strands S2 and S3 partially splay apart, disrupting the continuous H-bonding pattern. In DO, S3 is closer to S2 allowing canonical antiparallel H-bonding, and the sheet is extended with a strand from DMα96-99 (blue). (C) Alteration in the 3_{10} helix and adjacent extended strand. In DO, the extended region includes residues α49-60 (green). In DR both 3_{10} and α1 helices are longer by approximately one turn and the extended region corresponds to residues α51-56. The side chains of DO residues αF51 and αW43 are flipped

away from the rest of the structure and fit into pockets in DM, and the side chain of residue αF54 occupies the position corresponding to the MHCII P1 pocket. In DR these residues are found tucked into the structure in a different arrangement that lines the P1 peptide-side chain binding pocket. (D) Subunit interface in the center of the beta-sheet platform of DO in the region around Pα10a where a β-bulge is formed. The bulge is present in DO, absent in DR1, and present in DQ1 but with an additional H-bond.

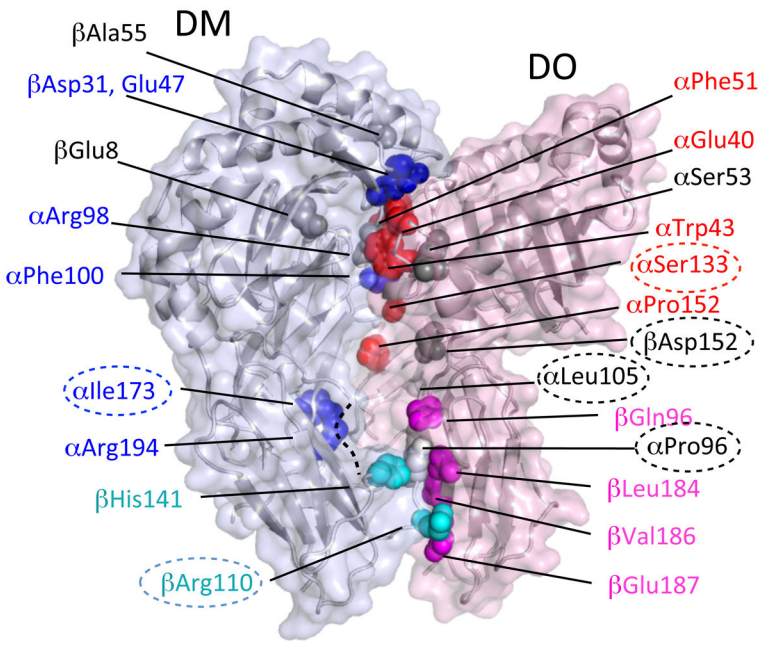

Figure 4. Mutations that alter DM-MHCII interaction map to the DO–DM interface

(A) DM point mutations and DR point mutations that interfere with peptide-exchange catalysis are shown mapped on the DO–DM crystal structure. Mutations that are found at the DO–DM interface are colored by domain; mutations not directly involved in the interface are colored gray. Most mutations that disrupt DM-MHCII interaction map to the same interface observed in the DM-DO crystal structure. *Dashes lines* encircle neoglycosylation mutations.

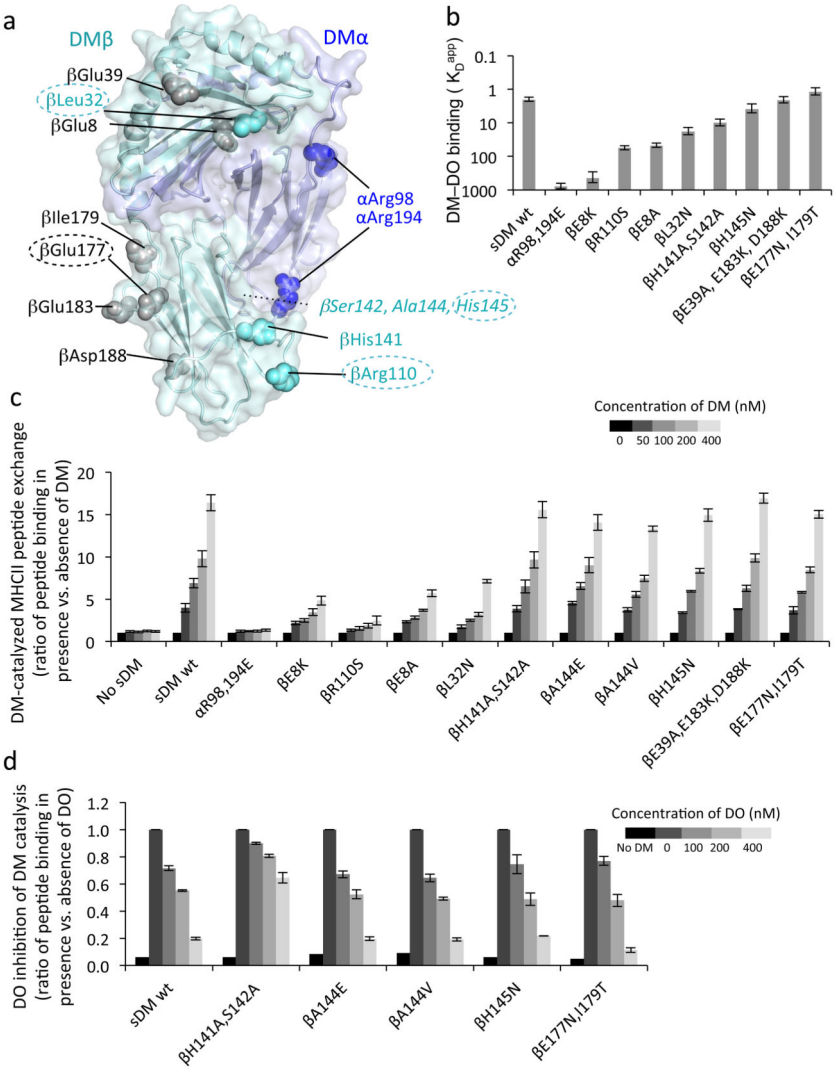

Figure 5. DM mutations at the DO interface have similar effects on interaction with DR and DO

(A) DM mutants investigated, representation as in Figure 4. (B) K_D^{app} data for mutant sDM binding to immobilized bio-szDOv. K_D^{app} for szDOv binding to immobilized bio-sDM is equivalent to wild type sDM binding to immobilized szDOv (not shown). (C) DM-mediated enhancement of peptide exchange to sDR4. sDR4-CLIP (10 nM) and biotinylated HA peptide (10 μM) were incubated with or without various concentrations of wild-type or mutant sDM. Peptide exchange levels, represented by the signal from bound HA, were normalized to the value observed without sDM. (D) Inhibition of DM-mediated peptide loading enhancement by DO. sDR4-CLIP and biotinylated HA were incubated with or without the maximum amount of sDM or sDM mutants used in panel C, in the presence of various concentrations of szDOv. Peptide exchange levels in each set were normalized to the value observed for corresponding sDM-only condition. Error bars show standard deviations from one experiment performed in triplicate and are representative of two or more experiments with similar results. Some data from mutants βH141A,S142A and βE177N, I179T have been reported [31], and are shown for comparison.

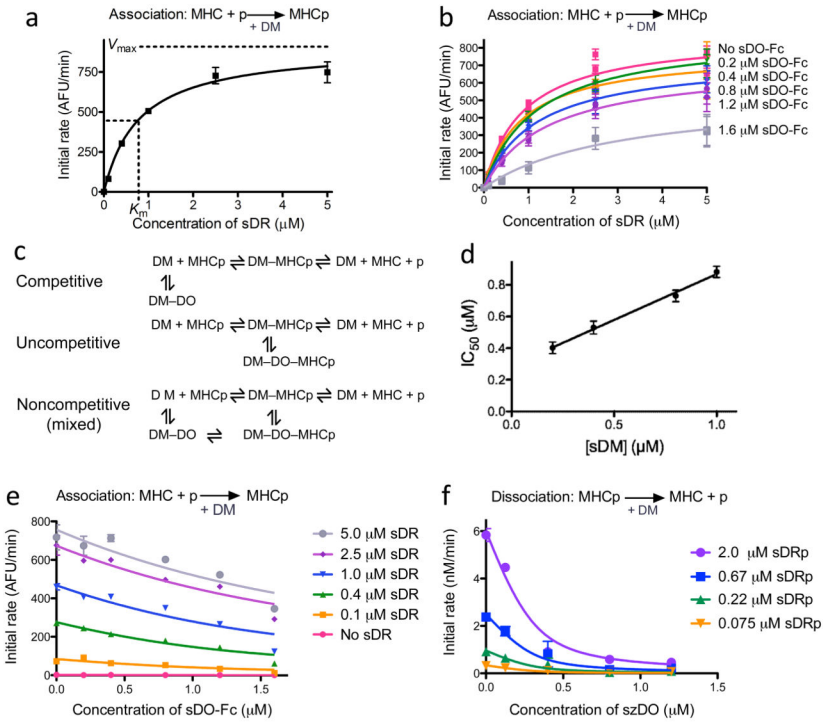

Figure 6. Kinetic analysis of DO inhibition of DM-catalyzed peptide exchange

(A.B) Michaelis-Menten analysis of sDM-catalyzed peptide binding to sDR1. (A) Initial rates from a catalyzed peptide dissociation experiment as shown in Fig 1e were fit to a hyperbolic equation (see Methods). Error bars show standard error (n=3). Data are representative of 3 experiments. (B) Kinetic parameters are altered in the presence of varying concentration of sDO-Fc. (C). Potential kinetic mechanisms for DO inhibition of DM-catalyzed peptide-MHC association or dissociation. See Methods for corresponding equations relating initial rates to the concentrations of sDM, sDR1, sDOv and values for K_m and model-dependent K_i^{app}. (D) sDM-catalyzed AMCA-HA peptide binding (0.08 μM) to sDR1 (0.5 μM) was measured in the presence of varying concentrations of sDO-Fc (0–2 μM) and sDM (0.2–1.0 μM). Linear dependence of IC_{50} on sDM reveals tight-binding inhibition. (E) sDM-catalyzed peptide binding to sDR was measured in the presence of varying concentrations of sDR1 (0.1–5μM) and sDO-Fc (0–1.6μM), 0.08μM AMCA-HA, and 0.4μM sDM. Data are representative of 3 experiments. (F) sDM-catalyzed peptide dissociation was measured for varying concentrations of Alexa-CLIP/sDR1 (0.075–2μM) in the presence of varying concentrations of sDOv (0–1.8μM), 12.5μM unlabeled HA peptide, and 0.3μM sDM. Values from two independent experiments are shown, with data representative of 4 experiments. In panels E and F, lines represent global fit to a competitive inhibition model.

Table 1

Data collection and refinement statistics (molecular replacement)

	HLA-DO – HLA-DM complex
Data collection	
Space group	$P2_1$
Cell dimensions	
a, *b*, *c* (Å)	83.26, 147.10, 95.96
α, β, γ (°)	90.00, 106.49, 90.00
Resolution (Å)	50 – 3.2 (3.26 – 3.20)
R_{sym}	19.6 (68.3)
R_{pim}[54]	11.4 (33.8)
$I/\sigma I$	5.4 (1.8)
Completeness (%)	94.0 (90.1)
Redundancy	3.8 (3.7)
Refinement	
Resolution (Å)	50.0–3.2
No. unique reflections	36,565
R_{work}/R_{free}	19.9/24.8
No. atoms	
Protein	11,996
Carbohydrate	260
Ligand/ion	49
Waters	8
Average *B*-factor (Å^2)	
Protein	49
Carbohydrate	65
Ligand/ion	16
Waters	6
R.m.s. deviations	
Bond lengths (Å)	0.004
Bond angles (°)	1.5